# Coupled systems of differential equations and chaos

Korsuize, A.E.

A.E. Korsuize

# Coupled systems of differential equations and chaos

Bachelorthesis, December 17, 2008

Supervisor: V. Rottschäfer

**Universiteit Leiden**

Mathematical Institute, Leiden University

**Abstract**

In this thesis we consider possible chaotic behavior of the stationary solutions of a coupled system of two partial differential equations. One of these PDE's is closely related to the complex Ginzburg-Landau equation; the other is a diffusion equation. First, some background and applications of this system are given. After rescaling and some simplifications, we uncouple the system and look at the solution structure of the separate parts. The part which is related to the Ginzburg-Landau equation contains, for a certain choice of coefficients, a homoclinic orbit. Then, we consider the coupled system and analyze what will happen to the homoclinic orbit. In order to do so, we recall the Melnikov theory, which is used to calculate the break up of the homoclinic orbit. If the Melnikov function equals zero and its derivative is nonzero, there will be a transverse homoclinic orbit. The existence of a transverse homoclinic orbit will give rise to chaotic behavior of the dynamical system and the theoretical background of this is described in detail. Finally, by applying the Melnikov theory to our system, we establish the possibility of a transverse homoclinic orbit and hence the possibility of chaos.

# Contents

# Chapter 1

# Introduction

## 1.1 The system

In this thesis we will study stationary solutions of the following system of partial differential equations:

$$
\begin{cases}
\frac{\partial A}{\partial t} = \alpha_1 \frac{\partial^2 A}{\partial x^2} + \alpha_2 A + \alpha_3 |A|^2 A + \mu AB \\[2mm]
\frac{\partial B}{\partial t} = \beta_1 \frac{\partial^2 B}{\partial x^2} + G(B, \frac{\partial B}{\partial x}, |A|^2)
\end{cases}
. \tag{1.1}
$$

Both $A$ and $B$ are complex amplitudes of the (real-valued) space variable $x$ and the (positive, real valued) time variable $t$. The coefficients $\alpha_i$ and $\beta_j$ will, in general, be complex-valued. $G$ is a function of $B$, $\frac{\partial B}{\partial x}$ and $|A|^2$.

Clearly, this is a coupled system, since the $A$-equation contains the $\mu AB$-term and the $B$-equation contains the $G$-function, which also depends on $A$.

Setting $\mu = 0$ makes the $A$-equation independent of $B$ and the remaining part is known as the complex Ginzburg-Landau (GL) equation. The GL equation is a generic amplitude equation that plays a role in various physical systems [1]. The $B$-equation can be thought of as a diffusion equation.

The coupled system (1.1) that is the subject of our study appears in several physical models of which we will give some examples in the following section.

## 1.2 Applications

A first example of a physical model where system (1.1) appears, is binary fluid convection.

Consider the following experimental setup. We take two, ideally infinitely long, plates with a liquid between them. We heat the bottom plate, while keeping the top plate at a constant temperature. We will now get a so-called convection flow. The basic principle is rather simple, the fluid at the bottom has a higher temperature, causing a lower density. The fluid at the top will keep a higher density and therefore, the top layer will start to sink, while the bottom layer will rise. When the colder fluid reaches the bottom, it will on its turn be heated up and start to rise. As a result we get a circular motion within the fluid. This motion is known as convection. See Figure 1.1 for an illustration. In a liquid consisting of just one substance, for example water, this convection forms stationary rolls. However, when the fluid is a binary fluid mixture, the rolls start to move. And not only that; all kinds of (local) patterns arise, see Figure 1.2. In order to study the rich behavior of this binary fluid convection, a model can be derived in which system (1.1) appears, see [9].

Another example comes from the geophysical morphodynamics, which studies the behavior of coastlines and sandbanks. In Figure 1.3 we see a map of the Wadden Isles. The isles seem to follow a certain pattern. Going from west to east, they start out rather big and decrease in size along the
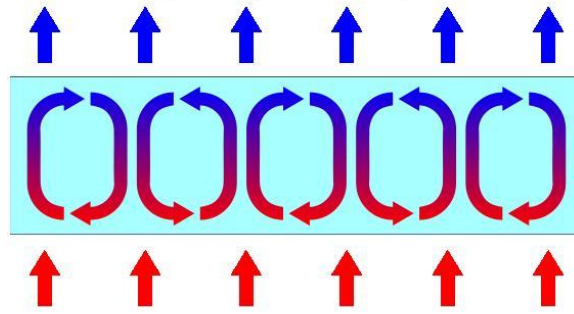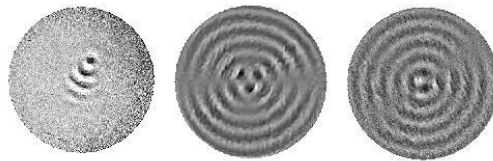
Figure 1.1: Convection flow



Figure 1.2: Binary Mixture Convection

coastline. They even disappear in the upward curve to the north. Then, going northward, they start to increase again. The formation of these isles and their developments are a result of the ebb tidal waves. In modeling this process, system (1.1) again plays a role, see [7].
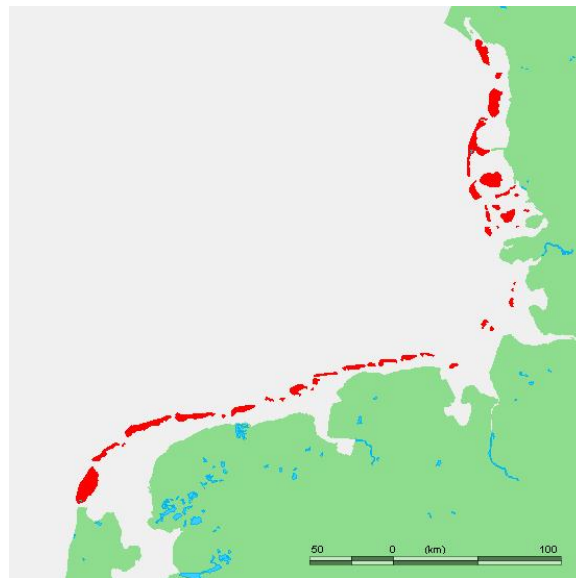


Figure 1.3: Wadden Isles

System (1.1) also arises in the study of nematic liquid crystals.
Liquid crystals are substances that exhibit a phase of matter that has properties between those of a conventional liquid, and those of a solid crystal. One of the most common liquid crystal phases is the nematic, where the molecules have no positional order, but they have long-range orientational order. Nematics have fluidity similar to that of ordinary (isotropic) liquids but they can be easily aligned by an external magnetic or electric field. An aligned nematic has optical properties which make them very useful in liquid crystal displays (LCD). An illustration of a liquid crystal in the nematic phase is

given in Figure 1.4. In studying these nematic liquid crystals, again, system (1.1) appears, see [5].



Figure 1.4: Nematic Liquid Chrystal

There are several other physical systems in which system (1.1) plays a role. The vast area of applications certainly justifies a thorough study of system (1.1) and a lot of work has already been done in [3, 4, 6]. In this thesis we will focus on possible chaotic behavior of system (1.1) and its underlying theory.
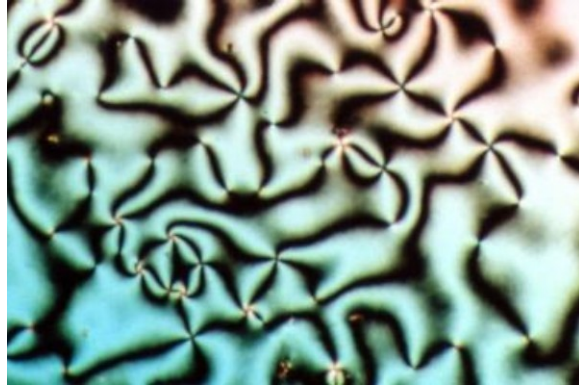
# Chapter 2

# Assumptions

In order to study system (1.1), we will make some assumptions which will simplify the analysis and give a better insight in the underlying mathematical complications. At a later stage, this study can be extended to include cases that we do not consider at the moment. For now, we will assume that:

- Both $A(x,t)$ and $B(x,t)$ are real valued functions

- All coefficients $\alpha_i$ and $\beta_j$ are real valued and nonzero

- The space variable $x$ is one dimensional

- For the function $G$ we take: $G(B, \frac{\partial B}{\partial x}, |A|^2) := \beta_2 B$

Note that by defining the $G$-function this way, the $B$-equation becomes independent of the $A$-equation. However, system (1.1) is still coupled by the $\mu$-term in the $A$-equation.

We will study stationary solutions of (1.1). Stationary solutions are solutions which remain constant over time, hence, all time-derivatives are equal to zero. Implementing this, leads to the following system:

$$\begin{cases} \alpha_1 \frac{\partial^2 A}{\partial x^2} + \alpha_2 A + \alpha_3 A^3 + \mu AB = 0 \\ \\ \beta_1 \frac{\partial^2 B}{\partial x^2} + \beta_2 B = 0 \end{cases} . \tag{2.1}$$

Note that all functions and coefficients in this system are real-valued.

# Chapter 3

# Rescaling

We will now rescale system (2.1). The basic principle of rescaling is to rewrite the system in other variables, without changing the behavior of the system. By choosing the scaling parameters in a smart way, we can reduce the number of coefficients.

We introduce scaling parameters $p, q, r \in \mathbb{R}$, such that: $p\widetilde{A} = A$, $q\widetilde{B} = B$ and $\widetilde{x} = rx$. $\widetilde{A}$ and $\widetilde{B}$ are the scaled amplitude functions and $\widetilde{x}$ is the scaled space variable. Rewriting (2.1) then yields:

$$\begin{cases} r^2 p \alpha_1 \frac{\partial^2 \widetilde{A}}{\partial \widetilde{x}^2} + p\alpha_2 \widetilde{A} + p^3 \alpha_3 \widetilde{A}^3 + pq\mu \widetilde{A}\widetilde{B} = 0 \\ \\ r^2 q \beta_1 \frac{\partial^2 \widetilde{B}}{\partial \widetilde{x}^2} + q\beta_2 \widetilde{B} = 0 \end{cases} . \tag{3.1}$$

For sake of an easier notation, we omit the tilde-signs and write the derivatives as a subscript. Rewriting the system gives:

$$\begin{cases} A_{xx} + \frac{\alpha_2}{\alpha_1 r^2} A + \frac{\alpha_3 p^2}{\alpha_1 r^2} A^3 + \frac{\mu q}{\alpha_1 r^2} AB = 0 \\ \\ B_{xx} + \frac{\beta_2}{\beta_1 r^2} B = 0 \end{cases} . \tag{3.2}$$

In order to keep the scaling parameter $r$ real valued, we choose $r^2 = \frac{\alpha_2}{\alpha_1}$ if $\frac{\alpha_2}{\alpha_1} > 0$ (case 1), and we take $r^2 = -\frac{\alpha_2}{\alpha_1}$ if $\frac{\alpha_2}{\alpha_1} < 0$ (case 2). This gives:

$$\begin{cases} A_{xx} \pm A \pm \frac{\alpha_3 p^2}{\alpha_2} A^3 \pm \frac{\mu q}{\alpha_2} AB = 0 \\ \\ B_{xx} + \frac{\beta_2}{\beta_1} |\frac{\alpha_1}{\alpha_2}| B = 0 \end{cases} . \tag{3.3}$$

In order to keep the parameter $p$ real valued, we choose $p^2 = \frac{\alpha_2}{\alpha_3}$ if $\frac{\alpha_3}{\alpha_2} > 0$ (case a), and we take $p^2 = -\frac{\alpha_2}{\alpha_3}$ if $\frac{\alpha_3}{\alpha_2} < 0$ (case b). Doing so, we get:

$$\begin{cases} A_{xx} \pm A \pm A^3 \pm \frac{\mu q}{\alpha_2} AB = 0 \\ \\ B_{xx} + \frac{\beta_2}{\beta_1} |\frac{\alpha_1}{\alpha_2}| B = 0 \end{cases} . \tag{3.4}$$

Finally, we choose $q = \alpha_1 r^2$ and introduce the coefficient $c = \frac{\beta_2}{\beta_1} |\frac{\alpha_1}{\alpha_2}|$ to obtain:

$$\begin{cases} A_{xx} \pm A \pm A^3 + \mu AB = 0 \\ \\ B_{xx} + cB = 0 \end{cases} . \tag{3.5}$$

The plus or minus signs depend on which case we consider.

# Chapter 4

# Analysis of the uncoupled system

After having made some assumptions and after rescaling, we have rewritten system (1.1) into (3.5). We will now thoroughly analyze this system. To do so, we first uncouple the system completely by setting $\mu = 0$ and look at the independent behavior of $A$ and $B$. Then, we will set $\mu \neq 0$ and look at the effect on the $A$-equation. In fact, the behavior of $A$ under coupling to $B$ is the basic subject of this thesis and we will discuss the underlying theory in the chapters to come. For now, we will first set $\mu = 0$ and look at the uncoupled system.

## 4.1 The B-equation

First, we consider the $B$-equation in system (3.5). This is a well known second order, homogeneous, ordinary differential equation. Its general solution is:

$B(x) = K_1 \sin x\sqrt{c} + K_2 \cos x\sqrt{c}$, for $c > 0$,

$B(x) = K_3 e^{x\sqrt{-c}} + K_4 e^{-x\sqrt{-c}}$, for $c < 0$ and

$B(x) = K_5 x + K_6$, for $c = 0$.

The $K_i$'s depend on initial conditions.

## 4.2 The A-equation

After setting $\mu = 0$ in system (3.5), the remaining part of the $A$-equation is a second order, homogeneous, ordinary differential equation: $A_{xx} \pm A \pm A^3 = 0$. We consider the four cases as described in chapter 3. First we rewrite this second order ODE into a system of first order ODE's. Define $z = A_x$ to obtain:

$$\begin{cases} A_x = z \\ z_x = \mp A \mp A^3 \end{cases}.$$

(4.1)

We determine the equilibrium points of (4.1) and classify them by calculating the Jacobian. The Jacobian in a point $(A, z)$ is given by:

$$J(A, z) = \begin{pmatrix} 0 & 1 \\ \mp 1 \mp 3A^2 & 0 \end{pmatrix}.$$

(4.2)

As said before, the plus or minus signs depend on which case we are considering.

## Case 1a

Case 1a: $(A_x = z; z_x = -A - A^3)$.
There's one equilibrium point at $(0,0)$ and the Jacobian is:
$J(0,0) = \begin{pmatrix} 0 & 1 \\ -1 & 0 \end{pmatrix}$ , hence $(0,0)$ is a center.
The phase portrait, including a typical trajectory, is given in Figure 4.1.



Figure 4.1: Case 1a

## Case 1b

Case 1b: $(A_x = z; z_x = -A + A^3)$.
There are three equilibrium points in this case, namely: $(0,0)$, $(1,0)$ and $(-1,0)$. The corresponding Jacobians are:
$J(0,0) = \begin{pmatrix} 0 & 1 \\ -1 & 0 \end{pmatrix} \Rightarrow$ Center, $J(\pm 1, 0) = \begin{pmatrix} 0 & 1 \\ 2 & 0 \end{pmatrix} \Rightarrow$ Saddle Points.
The phase portrait, including some possible trajectories, is given in Figure 4.2.



Figure 4.2: Case 1b

## Case 2a

Case 2a: $(A_x = z; z_x = A + A^3)$.
There's one equilibrium point at $(0,0)$ and the Jacobian is:

$$J(0,0) = \begin{pmatrix} 0 & 1 \\ 1 & 0 \end{pmatrix} \text{ , hence } (0,0) \text{ is a saddle point.}$$

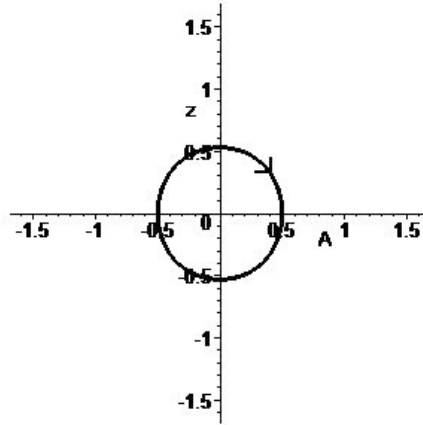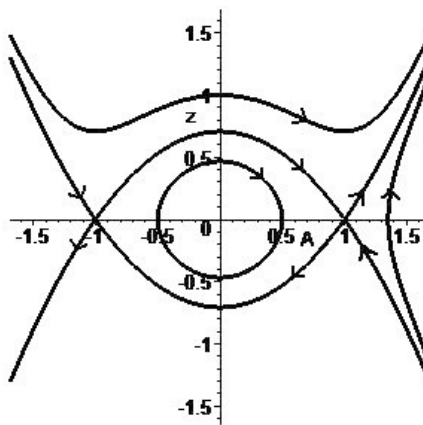The phase portrait, including some possible trajectories, is given in Figure 4.3.
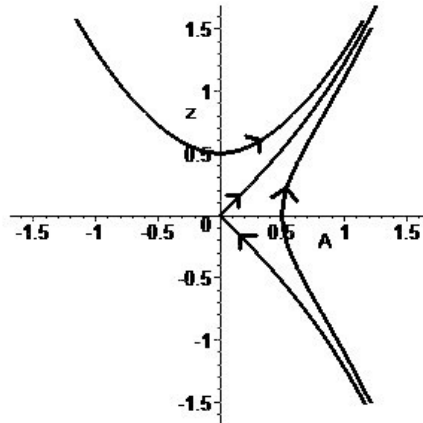


Figure 4.3: Case 2a

**Case 2b**

Case 2b: $(A_x = z; z_x = A - A^3)$.

There are three equilibrium points in this case, namely: $(0,0)$, $(1,0)$ and $(-1,0)$. The corresponding Jacobians are:

$$J(0,0) = \begin{pmatrix} 0 & 1 \\ 1 & 0 \end{pmatrix} \Rightarrow \text{Saddle Point, } J(\pm1,0) = \begin{pmatrix} 0 & 1 \\ -2 & 0 \end{pmatrix} \Rightarrow \text{Centers.}$$

The phase portrait and some trajectories are given in Figure 4.4.
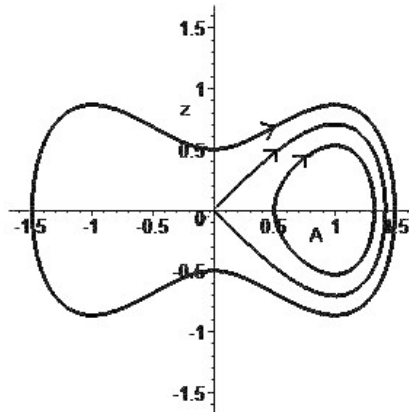


Figure 4.4: Case 2b

We will now consider case 2b in some more detail.

In the phase portrait (Figure 4.4) three possible trajectories (depending on initial values) are given. The trajectory which connects the point $(0,0)$ to itself describes the basic properties of the phase-plane. The saddle point $(0,0)$ is connected to itself by a so-called homoclinic orbit. This homoclinic orbit lies in the intersection of the stable and the unstable manifold of the equilibrium point $(0,0)$. The corresponding solution of the $A$-equation is a pulse solution, which can be determined explicitly: $A(x) = \sqrt{2}\text{sech}(x)$. See Figure 4.5 for a sketch of this pulse solution.

As $x \to -\infty$, $A(x) \to 0$ and $z(x) = \frac{d}{dx}A(x) \to 0$, which corresponds to the unstable manifold of
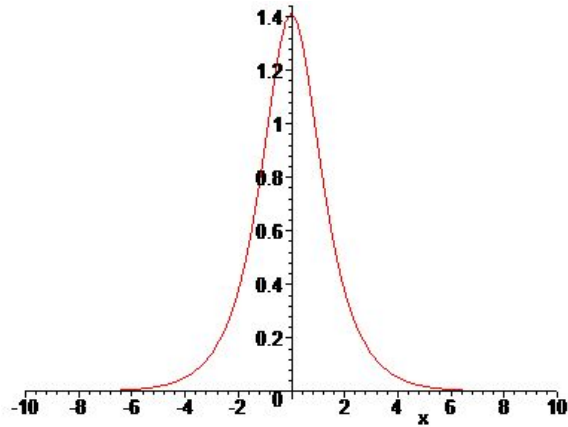
Figure 4.5: Pulse Solution

$(0, 0)$ in the phase-plane. Likewise, $A(x)$ and $z(x) = \frac{d}{dx} A(x)$ go to zero as $x \to \infty$, which corresponds to the stable manifold of $(0, 0)$.

## 4.3   Analysis of the coupled system

The question rises, what will happen to the case 2b when we take $\mu \neq 0$ in system (3.5). We expect that the homoclinic orbit will break open, i.e. the stable and unstable manifold of the point $(0, 0)$ will not longer coincide. Indeed, this will happen, but under certain conditions, the manifolds may still have an intersection in a point. As we will see, this results in possible chaotic behavior of this dynamical system. The underlying theory will be developed in the next chapters. In what follows, we assume that the coefficient $c$ from system (3.5) is greater than zero, which means (as explained in section 4.1) that the solution of the $B$-equation is given by:

$$B(x) = K_1 \sin x \sqrt{c} + K_2 \cos x \sqrt{c}. \tag{4.3}$$

And as a result, the $A$-equation for case 2b is then given by:

$$A_{xx} - A + A^3 + \mu A(K_1 \sin x \sqrt{c} + K_2 \cos x \sqrt{c}) = 0. \tag{4.4}$$

Or, rewritten into a system of first order ODE's, as done in section 4.2:

$$\begin{cases} A_x = z \\ z_x = A - A^3 - \mu A(K_1 \sin x \sqrt{c} + K_2 \cos x \sqrt{c}) \end{cases}. \tag{4.5}$$

# Chapter 5

# Melnikov theory

In order to determine what will happen to the phase-plane in Figure 4.4 when we set $\mu \neq 0$, we use Melnikov's method for homoclinic orbits. First, we will recall the general theory and later we will show that this theory can be applied to our system.

## 5.1 Necessary assumptions

Melnikov's theory is applicable to systems which can be written in the following way:

$$\begin{cases} \dot{x} = \frac{\partial H}{\partial y}(x,y) + \varepsilon g_1(x,y,t,\varepsilon) \\ \dot{y} = -\frac{\partial H}{\partial x}(x,y) + \varepsilon g_2(x,y,t,\varepsilon) \end{cases}, \tag{5.1}$$

where $(x,y) \in \mathbb{R}^2$. The dots indicate a derivative with respect to $t$. The function $H(x,y)$ is a Hamiltonian function. The parameter $\varepsilon$ is small and setting $\varepsilon = 0$ corresponds to the unperturbed system. We can write (5.1) in vector form as:

$$\dot{q} = JDH(q) + \varepsilon g(q,t,\varepsilon), \tag{5.2}$$

where $q = (x,y)$, $DH = (\frac{\partial H}{\partial x}, \frac{\partial H}{\partial y})$, $g = (g_1, g_2)$, and

$$J = \begin{pmatrix} 0 & 1 \\ -1 & 0 \end{pmatrix}.$$

Furthermore, we make the following assumptions:

- System (5.1) is sufficiently differentiable on the region of interest

- The perturbation function $g = (g_1, g_2)$ is periodic in $t$ with period $T = \frac{2\pi}{\omega}$

- The unperturbed system possesses a hyperbolic fixed point, $p_0$, connected to itself by a homoclinic orbit $q_0(t) = (x_0(t), y_0(t))$

- The region of the phase plane which is enclosed by the homoclinic orbit possesses a continuous family of periodic orbits

Before proceeding, we rewrite (5.1) as an autonomous three dimensional system:

$$\begin{cases} \dot{x} = \frac{\partial H}{\partial y}(x,y) + \varepsilon g_1(x,y,\phi,\varepsilon) \\ \dot{y} = -\frac{\partial H}{\partial x}(x,y) + \varepsilon g_2(x,y,\phi,\varepsilon) \\ \dot{\phi} = \omega \end{cases}, \tag{5.3}$$
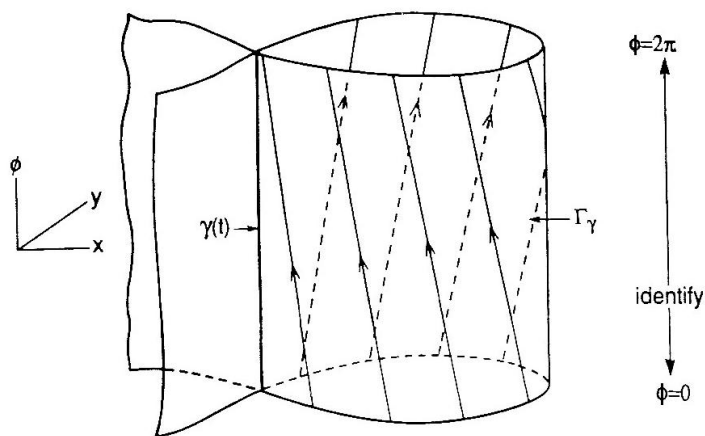
Figure 5.1: Homoclinic Manifold[11]

where $(x, y, \phi) \in \mathbb{R}^2 \times \mathrm{S}^1$.

First, we take a look at the unperturbed system ($\varepsilon = 0$), see Figure 5.1. When viewed in the three dimensional phase space $\mathbb{R}^2 \times \mathrm{S}^1$, the hyperbolic fixed point $p_0$ becomes a periodic orbit $\gamma(t) = (p_0, \phi(t))$, where $\phi(t) = \omega t + \phi_0$. We denote the two-dimensional stable and unstable manifolds of $\gamma(t)$ by $W^s(\gamma(t))$ and $W^u(\gamma(t))$. These two manifolds coincide along a two dimensional homoclinic manifold, which we call $\Gamma_\gamma$.

When we set $\varepsilon \neq 0$, $W^s(\gamma(t))$ and $W^u(\gamma(t))$ will most probably not longer coincide and we get a three dimensional phase space which looks like Figure 5.2.

Our goal is to analytically quantify Figure 5.2, by developing a measurement of the deviation of
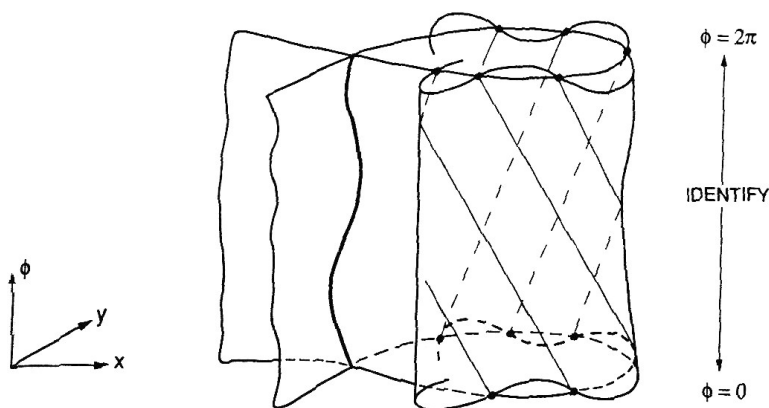


Figure 5.2: Perturbed Homoclinic Manifold[11]

$W^s(\gamma(t))$ and $W^u(\gamma(t))$ from $\Gamma_\gamma$. This deviation will probably depend on the place on $\Gamma_\gamma$ where we measure it, so we will first describe a parametrization of $\Gamma_\gamma$.

## 5.2 Parametrization of the homoclinic manifold of the unperturbed system

Consider a point $p \in \Gamma_\gamma$. This point lies in the three dimensional space $(x, y, \phi) \in \mathbb{R}^2 \times \mathrm{S}^1$.

The homoclinic orbit of the unperturbed two dimensional system is given by $q_0(t) = (x_0(t), y_0(t))$. For $t \to -\infty \Rightarrow q_0(t) \to p_0$ (the unstable manifold) and for $t \to \infty \Rightarrow q_0(t) \to p_0$ (the stable manifold). For $t = 0$ we have the initial value $q_0(0) = (x_0(0), y_0(0))$. Every point $q$ on this homoclinic orbit can be given by an unique $t_0$: $q = q_0(-t_0)$, where $t_0$ can be interpreted as the time of flight from the point $q_0(-t_0)$ to the point $q_0(0)$.

Every point $p \in \Gamma_\gamma$ with coordinates $(x_p, y_p, \phi_p)$ can then be represented as $(q_0(-t_0), \phi_0)$, with $t_0 \in \mathbb{R}$ and $\phi_0 \in (0, 2\pi]$.

In every point $p \in \Gamma_\gamma$ we can define a normal vector:

$$\pi_p = (\frac{\partial H}{\partial x}(x_0(-t_0), y_0(-t_0)), \frac{\partial H}{\partial y}(x_0(-t_0), y_0(-t_0)), 0). \tag{5.4}$$

We may also write this as: $\pi_p = (DH(q_0(-t_0)), 0)$, see Figure 5.3.



Figure 5.3: Normal Vector in the point $p$[11]

## 5.3 Phase space geometry of the perturbed system
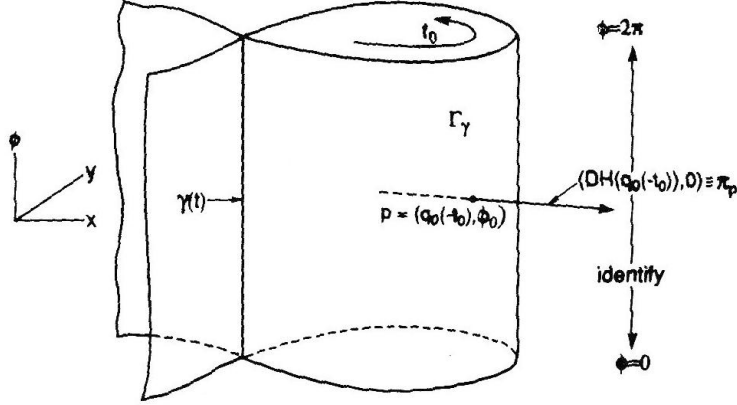
We will now look at the result of setting $\varepsilon \neq 0$. Firstly, we note that, for $\varepsilon$ sufficiently small, the periodic orbit $\gamma(t)$ (from the unperturbed system) persists as a periodic orbit in the perturbed system: $\gamma_\varepsilon(t) = \gamma(t) + O(\varepsilon)$. This periodic orbit $\gamma_\varepsilon(t)$ has the same stability type as $\gamma(t)$ and the local manifolds $W^s_{loc}(\gamma_\varepsilon(t))$ and $W^u_{loc}(\gamma_\varepsilon(t))$ are $\varepsilon$-close to $W^s_{loc}(\gamma(t))$ and $W^u_{loc}(\gamma(t))$ respectively[11].

If $\Phi_t(\cdot)$ denotes the flow generated by system (5.3), then we define the global stable and unstable manifolds of $\gamma_\varepsilon(t)$ as:

$$W^s(\gamma_\varepsilon(t)) = \bigcup_{t \leq 0} \Phi(W^s_{loc}(\gamma_\varepsilon(t))) \; ; \; W^u(\gamma_\varepsilon(t)) = \bigcup_{t \geq 0} \Phi(W^u_{loc}(\gamma_\varepsilon(t))). \tag{5.5}$$

When we look at the perturbed system, the normal vector $\pi_p$ in point $p \in \Gamma_\gamma$ (as defined in (5.4)) will intersect the global stable and unstable manifolds of $\gamma_\varepsilon(t)$ in the points $p^s_\varepsilon$ and $p^u_\varepsilon$ respectively, see Figure 5.4.

The distance between $W^s(\gamma_\varepsilon(t))$ and $W^u(\gamma_\varepsilon(t))$ at the point $p$ is then defined to be:

$$d(p, \varepsilon) = |p^u_\varepsilon - p^s_\varepsilon|. \tag{5.6}$$

An equivalent way of defining the distance between the manifolds is:

$$d(p, \varepsilon) = \frac{(p^u_\varepsilon - p^s_\varepsilon) \cdot \pi_p}{||\pi_p||}. \tag{5.7}$$

Since $p^u_\varepsilon$ and $p^s_\varepsilon$ are chosen to lie on $\pi_p$, the magnitude of (5.6) and (5.7) is exactly equal. Also, because $\pi_p$ is parallel to the $xy$-plane, $p^u_\varepsilon$ and $p^s_\varepsilon$ will have the same $\phi$-coordinate as $p$; $p^u_\varepsilon = (q^u_\varepsilon, \phi_0)$ and $p^s_\varepsilon = (q^s_\varepsilon, \phi_0)$. Using this and the fact that $\pi_p$ can be written as $(DH(q_0(-t_0)), 0)$, we can now rewrite expression (5.7) as:

$$d(p, \varepsilon) = \frac{(p^u_\varepsilon - p^s_\varepsilon) \cdot \pi_p}{||\pi_p||} = \frac{((q^u_\varepsilon, \phi_0) - (q^s_\varepsilon, \phi_0)) \cdot (DH(q_0(-t_0)), 0)}{||(DH(q_0(-t_0)), 0)||} = \frac{DH(q_0(-t_0)) \cdot (q^u_\varepsilon - q^s_\varepsilon)}{||DH(q_0(-t_0))||}. \tag{5.8}$$
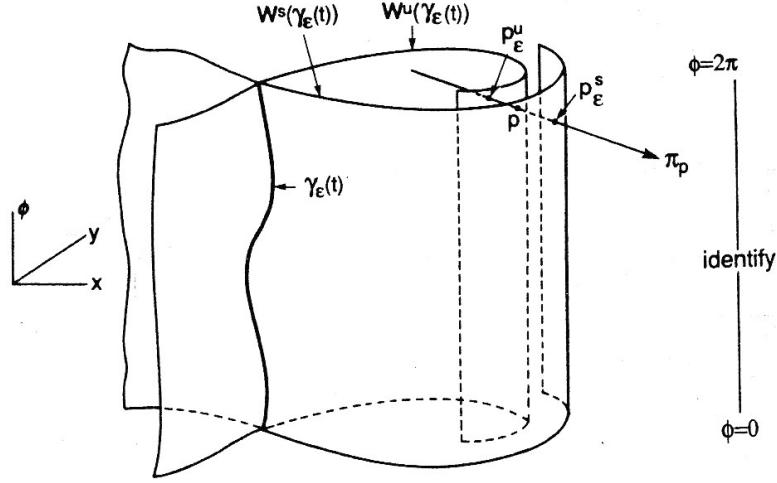
Figure 5.4: Normal Vector in Perturbed Manifold[11]

Notice that in fact we should now write $d(t_0, \phi_0, \varepsilon)$ instead of $d(p, \varepsilon)$, since $p$ has disappeared on the right hand side of the equation. However, since every $p \in \Gamma_\gamma$ can be uniquely represented by the parameters $t_0$ and $\phi_0$, we leave it as it is.

## 5.4 Derivation of the Melnikov function

A Taylor expansion of (5.8) about $\varepsilon = 0$ gives:

$$d(p, \varepsilon) = d(t_0, \phi_0, \varepsilon) = d(t_0, \phi_0, 0) + \varepsilon \frac{\partial d}{\partial \varepsilon}(t_0, \phi_0, 0) + \mathcal{O}(\varepsilon^2). \tag{5.9}$$

Since the stable and unstable manifolds coincide for $\varepsilon = 0$, we have $d(t_0, \phi_0, 0) = 0$. The remaining part is:

$$d(t_0, \phi_0, \varepsilon) = \varepsilon \frac{\partial d}{\partial \varepsilon}(t_0, \phi_0, 0) + \mathcal{O}(\varepsilon^2) = \varepsilon \frac{M(t_0, \phi_0)}{||DH(q_0(-t_0))||} + \mathcal{O}(\varepsilon^2), \tag{5.10}$$

where $M(t_0, \phi_0)$ is the so-called Melnikov function, defined to be:

$$M(t_0, \phi_0) = DH(q_0(-t_0)) \cdot \left( \frac{\partial q_\varepsilon^u}{\partial \varepsilon}|_{\varepsilon=0} - \frac{\partial q_\varepsilon^s}{\partial \varepsilon}|_{\varepsilon=0} \right). \tag{5.11}$$

We will now show that it is possible to find an expression for (5.11) without having any information on what the perturbed manifolds look like. This smart method is due to and called after the Russian mathematician Melnikov.

Firstly, we define the time dependent Melnikov function:

$$M(t; t_0, \phi_0) = DH(q_0(t - t_0)) \cdot \left( \frac{\partial q_\varepsilon^u(t)}{\partial \varepsilon}|_{\varepsilon=0} - \frac{\partial q_\varepsilon^s(t)}{\partial \varepsilon}|_{\varepsilon=0} \right), \tag{5.12}$$

where $q_0(t - t_0)$ is the unperturbed homoclinic orbit and $q_\varepsilon^u(t)$ and $q_\varepsilon^s(t)$ are the orbits in the perturbed unstable and stable manifolds $W^u(\gamma_\varepsilon(t))$ and $W^s(\gamma_\varepsilon(t))$ respectively. For $t = 0$ we have the expression as defined in (5.11).

We will now derive a differential equation that $M(t; t_0, \phi_0)$ must satisfy. For the sake of an easier notation we define:

$$q_1^{u,s}(t) = \frac{\partial q_\varepsilon^{u,s}(t)}{\partial \varepsilon}|_{\varepsilon=0} \tag{5.13}$$

and

$$\Delta^{u,s}(t) = DH(q_0(t - t_0)) \cdot q_1^{u,s}(t), \tag{5.14}$$

so that (5.12) becomes:
$$M(t; t_0, \phi_0) = \Delta^u(t) - \Delta^s(t). \tag{5.15}$$

Differentiating (5.14), with respect to $t$, gives:

$$\frac{d}{dt}(\Delta^{u,s}(t)) = (\frac{d}{dt}(DH(q_0(t - t_0)))) \cdot q_1^{u,s}(t) + DH(q_0(t - t_0)) \cdot \frac{d}{dt}q_1^{u,s}(t). \tag{5.16}$$

Now we have to realize that $q_\varepsilon^{u,s}(t)$, appearing in (5.13) are the orbits in the perturbed manifolds and should therefore satisfy the differential equation (5.2). This is because $q_\varepsilon^{u,s}(t)$ are solutions of the perturbed system. Hence:

$$\frac{d}{dt}(q_\varepsilon^{u,s}(t)) = JDH(q_\varepsilon^{u,s}(t)) + \varepsilon g(q_\varepsilon^{u,s}(t), \phi(t), \varepsilon). \tag{5.17}$$

Differentiating (5.17) with respect to $\varepsilon$ yields the so called first variational equation:

$$\frac{d}{dt}q_1^{u,s}(t) = JD^2H(q_0(t - t_0))q_1^{u,s}(t) + g(q_0(t - t_0), \phi(t), 0). \tag{5.18}$$

For a more detailed version of the derivation of this first variational equation, we refer to Wiggins[11]. Substituting (5.18) into (5.16) gives, after some cumbersome calculation, the following expression:

$$\frac{d}{dt}(\Delta^{u,s}(t)) = DH(q_0(t - t_0)) \cdot g(q_0(t - t_0), \phi(t), 0). \tag{5.19}$$

Integrating $\Delta^u(t)$ and $\Delta^s(t)$ from $-\tau$ to 0 and 0 to $\tau$ ($\tau > 0$) gives:

$$\Delta^u(0) - \Delta^u(-\tau) = \int_{-\tau}^0 (DH(q_0(t - t_0)) \cdot g(q_0(t - t_0), \phi(t), 0))dt \tag{5.20}$$

and

$$\Delta^s(\tau) - \Delta^s(0) = \int_0^\tau (DH(q_0(t - t_0)) \cdot g(q_0(t - t_0), \phi(t), 0))dt. \tag{5.21}$$

Using this, the Melnikov function now becomes:

$$M(t_0, \phi_0) = M(0; t_0, \phi_0) = \Delta^u(0) - \Delta^s(0) = \int_{-\tau}^\tau (DH(q_0(t-t_0)) \cdot g(q_0(t-t_0), \omega t + \phi_0, 0))dt + \Delta^s(\tau) - \Delta^u(-\tau). \tag{5.22}$$

When considering the limit of (5.22) for $\tau \to \infty$, we get the following results:

- $\lim_{\tau \to \infty} \Delta^s(\tau) = \lim_{\tau \to \infty} \Delta^u(-\tau) = 0$
- The improper integral $\int_{-\infty}^\infty (DH(q_0(t - t_0)) \cdot g(q_0(t - t_0), \omega t + \phi_0, 0))dt$ converges absolutely

For a proof of these two results, we refer to Wiggins[11]. Implementing these results into (5.22), yields:

$$M(t_0, \phi_0) = \int_{-\infty}^\infty (DH(q_0(t - t_0)) \cdot g(q_0(t - t_0), \omega t + \phi_0, 0))dt. \tag{5.23}$$

Or equivalently, after making the transformation $t \mapsto t + t_0$:

$$M(t_0, \phi_0) = \int_{-\infty}^\infty (DH(q_0(t)) \cdot g(q_0(t), \omega t + \omega t_0 + \phi_0, 0))dt. \tag{5.24}$$

We have hence obtained a computable expression for the Melnikov function $M(t_0, \phi_0)$. Since, by assumption, the function $g(q, \cdot, 0)$ is periodic, the Melnikov function will be periodic in $t_0$ and in $\phi_0$. Considering expression (5.24), it is clear that varying $t_0$ or $\phi_0$ have the same effect. This will be further explained in section 6.1.

# Chapter 6

# Transverse homoclinic orbit

Now that we have derived a computable expression of the Melnikov function (5.24), we pay attention to a particular situation, namely the case in which the Melnikov function equals zero. We recall that the distance between the stable and unstable manifold in the perturbed system (5.3) is given by expression (5.10). Since $DH(q_0(-t_0))$ is nonzero for $t_0$ finite, $M(t_0, \phi_0) = 0$ implies that $d(t_0, \phi_0, \varepsilon) = 0$. In other words, if the Melnikov function equals zero, the stable and unstable manifold will intersect. If the derivative of $M(t_0, \phi_0)$ with respect to $t_0$ (or equivalently with respect to $\phi_0$) is nonzero, this intersection will be transversal [11].

## 6.1 Poincaré map

The Poincaré map is a basic tool in studying the stability and bifurcations of periodic orbits. The idea of the Poincaré map is as follows: If $\Gamma$ is a periodic orbit of the system $\dot{x} = f(x)$ through the point $x_0$ and $\Sigma$ is a hyperplane transverse to $\Gamma$ at $x_0$, then for any point $x \in \Sigma$ sufficiently near $x_0$, the solution of $\dot{x} = f(x)$ through $x$ at $t = 0$, $\Phi_t$, will cross $\Sigma$ again at a point $P(x)$ near $x_0$, see Figure 6.1. The mapping $x \to P(x)$ is called the Poincaré map.
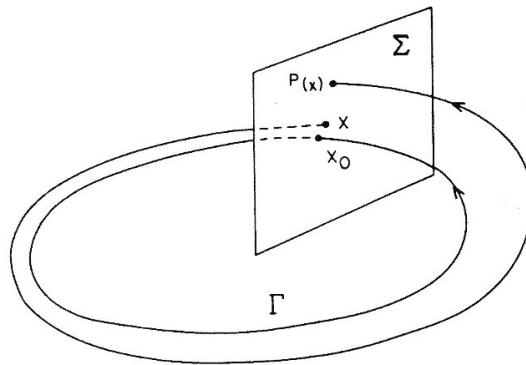


Figure 6.1: The Poincaré map[8]

When observing the phase space of the perturbed vector field in Figure 5.2, we can define a cross-section:

$$\Sigma^{\phi_0} = \{(q, \phi) \in \mathbb{R}^2 \times S^1 | \phi = \phi_0\}. \tag{6.1}$$

Since $\dot{\phi} = \omega \geq 0$, the vector field is transverse to $\Sigma^{\phi_0}$. The Poincaré map of $\Sigma^{\phi_0}$ to itself, defined by the flow of the vector field, is then given by:

$$P_\varepsilon : \Sigma^{\phi_0} \to \Sigma^{\phi_0} \; ; \; q_\varepsilon(0) \mapsto q_\varepsilon(2\pi/\omega). \tag{6.2}$$

The periodic orbit $\gamma_\varepsilon$ intersects $\Sigma^{\phi_0}$ in a point $p_{\varepsilon,\phi_0}$. This point is a hyperbolic fixed point for the defined Poincaré map. It has a one-dimensional stable and unstable manifold given by:

$$W^{s,u}(p_{\varepsilon,\phi_0}) = W^{s,u}(\gamma_\varepsilon) \cap \Sigma^{\phi_0}. \tag{6.3}$$

As we have already mentioned, the manifolds will intersect transversally when the Melnikov function equals zero and its derivative is nonzero. The Poincaré map gives a geometrical interpretation of this. Fixing $\phi_0$ and varying $t_0$ corresponds to fixing the cross-section $\Sigma^{\phi_0}$ and measuring the distance between the manifolds for different values of $t_0$. If for some value of $t_0$ the Melnikov function equals zero and its derivative with respect to $t_0$ is nonzero, the manifolds will intersect transversally. Likewise, fixing $t_0$ and varying $\phi_0$ corresponds to fixing $\pi_p$ at a specific point $(q_0(-t_0), \phi_0)$ on $\Gamma_\gamma$ and measuring the distance between the manifolds for different values of $\phi_0$, i.e. on different cross-sections $\Sigma^{\phi_0}$. If the Melnikov function equals zero for some value $\phi_0$ and its derivative with respect to $\phi_0$ is nonzero, we have a transversal intersection of the manifolds.

## 6.2   Homoclinic tangle

Suppose that for some value $\phi_0$, or equivalently $t_0$, the Melnikov function equals zero and its derivative is nonzero. The cross-section $\Sigma^{\phi_0}$, then looks like illustrated in Figure 6.2. The hyperbolic fixed point
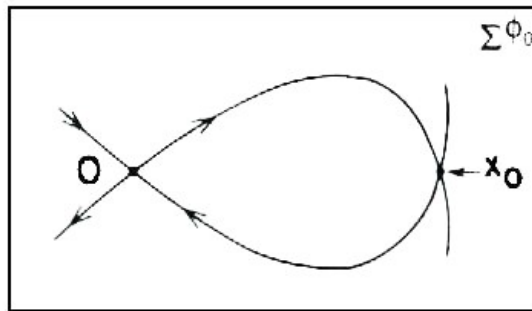


Figure 6.2: Transversal intersection of the manifolds[11]

of the Poincaré map, $p_{\varepsilon,\phi_0}$, is called 0 here and the point where the manifolds intersect is called $x_0$. The fixed point 0 is, by definition, invariant under $P_\varepsilon$. For iterates of $x_0$ under $P_\varepsilon$, we have to realize that $x_0$ is both in the stable and unstable manifold: $x_0 \in W^s(0) \cap W^u(0)$. Since $W^s(0)$ and $W^u(0)$ are invariant under $P_\varepsilon$, the iterates $\{...P_\varepsilon^{-2}(x_0), P_\varepsilon^{-1}(x_0), P_\varepsilon^1(x_0), P_\varepsilon^2(x_0)...\}$ also lie in $W^s(0) \cap W^u(0)$. This leads to a so-called homoclinic tangle, wherein $W^s(0)$ and $W^u(0)$ accumulate on themselves, see Figure 6.3

The dynamics in this homoclinic tangle exhibit chaotical behavior. This will be explained in the following chapters.

Figure 6.3: The homoclinic tangle[8]

# Chapter 7

# Smale Horseshoe

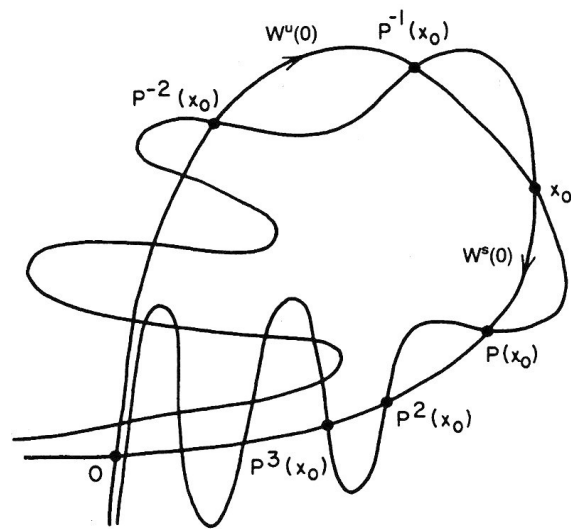To understand the dynamics in the homoclinic tangle as illustrated in Figure 6.3, we first have to study the so called Smale Horseshoe Map (SHM). This map has some very interesting properties which will turn out to be closely related to the dynamics in the homoclinic tangle.

## 7.1 Definition of the Smale Horseshoe Map

We begin with the unit square $S = [0, 1] \times [0, 1]$ in the plane and define a mapping $f : S \to \mathbb{R}^2$ as follows: the square is contracted in in the $x$-direction by a factor $\lambda$, expanded in the $y$-direction by a factor $\mu$ and then folded around, laying it back on the square as shown in Figure 7.1.

We only take into account the part of $f(S)$ that again is contained in $S$. Consider two horizontal
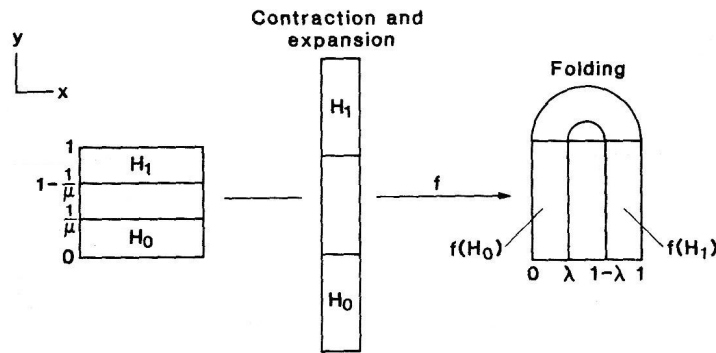


Figure 7.1: The Smale Horseshoe[11]

rectangles $H_0$ and $H_1 \in S$ defined as:

$$H_0 = \{(x,y) \in \mathbb{R}^2 | 0 \leq x \leq 1, 0 \leq y \leq \frac{1}{\mu}\}, \ H_1 = \{(x,y) \in \mathbb{R}^2 | 0 \leq x \leq 1, 1 - \frac{1}{\mu} \leq y \leq 1\}, \qquad (7.1)$$

with $\mu > 2$.
Then $f$ maps these to two vertical rectangles $V_0$ and $V_1 \in S$:

$$f(H_0) = V_0 = \{(x,y) \in \mathbb{R}^2 | 0 \leq x \leq \lambda, 0 \leq y \leq 1\}, \ f(H_1) = V_1 = \{(x,y) \in \mathbb{R}^2 | 1 - \lambda \leq x \leq 1, 0 \leq y \leq 1\},$$
$$(7.2)$$

with $0 < \lambda < \frac{1}{2}$.
The horizontal strip in $S$ between $H_0$ and $H_1$ is the folding section and its image under $f$ falls outside

$S$. In matrix notation the map $f$ on $H_0$ and $H_1$ is given by:

$$H_0 : \begin{pmatrix} x \\ y \end{pmatrix} \mapsto \begin{pmatrix} \lambda & 0 \\ 0 & \mu \end{pmatrix} \begin{pmatrix} x \\ y \end{pmatrix}, H_1 : \begin{pmatrix} x \\ y \end{pmatrix} \mapsto \begin{pmatrix} -\lambda & 0 \\ 0 & -\mu \end{pmatrix} \begin{pmatrix} x \\ y \end{pmatrix} + \begin{pmatrix} 1 \\ \mu \end{pmatrix}, \qquad (7.3)$$

with $0 < \lambda < \frac{1}{2}$, $\mu > 2$.

The inverse map $f^{-1}$ works as illustrated in Figure 7.2.
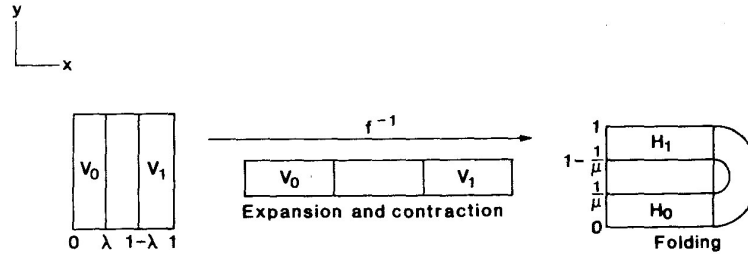


Figure 7.2: The Inverse Smale Horseshoe[11]

Under $f^{-1}$ vertical rectangles in $S$ are mapped to horizontal rectangles in $S$. Again, the folding section falls outside $S$.

When $f$ is applied to a vertical rectangle $V \in S$, then $f(V) \cap S$ consists of two vertical rectangles, one in $V_0$ and one in $V_1$, both with width being equal to the factor $\lambda$ times the width of $V$. Likewise, when $f^{-1}$ is applied to a horizontal rectangle $H \in S$, $f^{-1}(H) \cap S$ consists of two horizontal rectangles, one in $H_0$ and one in $H_1$, both with width equal to $\mu$ times the width of $H$, see Figure 7.3.
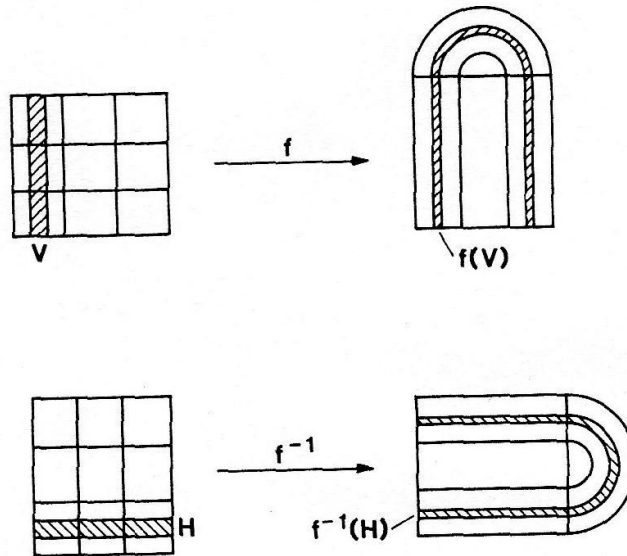


Figure 7.3: The Smale Horseshoe Map on horizontal and vertical rectangles[11]

## 7.2 Invariant set

When we apply $f$ and/or $f^{-1}$ many times, most points will eventually leave $S$. We are interested in the points (if any), which stay in $S$ for all iterations of $f$. These points form the invariant set of the

SHM. The invariant set $\Lambda$ is defined as: $\Lambda = \bigcap_{n=-\infty}^{\infty} f^n(S)$.

This invariant set can be constructed in a inductively way for both the positive and negative iterates of $f$. First we look at the positive iterates and determine what happens to $f^k$ when $k \to \infty$. Then we will do the same for $k \to -\infty$.

We start with the positive iterates. By definition of $f$, $S \cap f(S)$ consists of two vertical rectangles $V_0$ and $V_1$, both with width $\lambda$. As explained in section 7.1, $S \cap f(S) \cap f^2(S)$ will then exist of four vertical rectangles, two in $V_0$ and two in $V_1$, each with widths $\lambda^2$. See Figure 7.4.

In order to keep track of what happens to all the rectangles under iterations of $f$, we introduce the
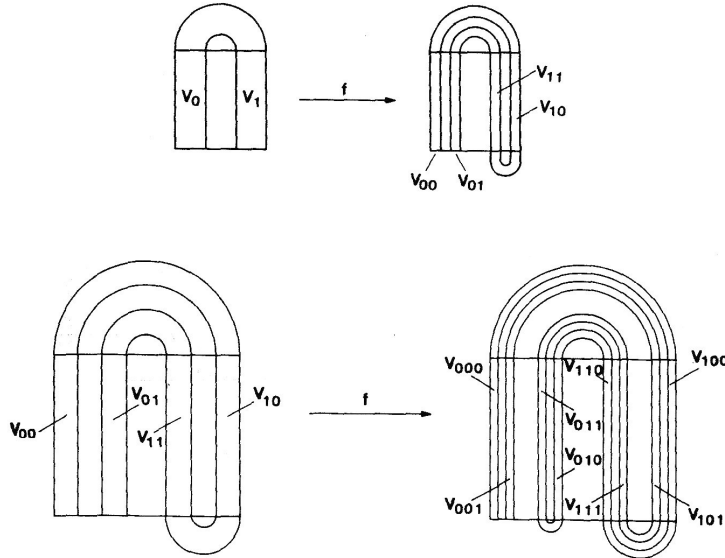


Figure 7.4: Positive iterates[11]

following notation: $V_{ij}$, with $i, j \in \{0, 1\}$ means: the rectangle is situated in $V_i$ (left rectangle for $i = 0$ and right for $i = 1$) and its pre-image was situated in $V_j$ ($f^{-1}(V_{ij}) \in V_j$). In Figure 7.4 for example, $V_{01}$ is situated in $V_0$ and $f^{-1}(V_{01})$ lies in $V_1$.

We can now continue this induction process of $f^k(S)$ for $k = 3, 4...$ See Figure 7.4 for an illustration of $S \cap f(S) \cap f^2(S) \cap f^3(S)$.

We get $2^3 = 8$ rectangles, each of width $\lambda^3$. Two rectangles are situated in $V_{00}$, two in $V_{01}$ etc. Again we can number all the rectangles by an unique label: $V_{pq}$, with $p \in \{0, 1\}; q \in \{0, 1\}^2$, meaning: the rectangle is now situated in $V_p$ and its pre-image is in $V_q$ (which in turn can be written as $V_q = V_{ij}$). In Figure 7.4, for example, the rectangle $V_{101}$ is situated in $V_1$ (the righthand side of $S$) and $f^{-1}(V_{101})$ lies in rectangle $V_{01}$.

When we continue the process for increasing $k$, we have, at the $k$-th stage, $2^k$ vertical rectangles, all with an unique label from the collection $\{0, 1\}^k$ and all with width $\lambda^k$. When $k \to \infty$, we end up with an infinite number of vertical rectangles, which are in fact vertical lines, as $\lim_{k\to\infty} \lambda^k = 0$ (remember that $0 < \lambda < \frac{1}{2}$). All these lines have a unique label which consists of an infinite series of 0's and 1's.

Now we turn to the negative iterates of $f$. In fact the procedure is analogue to the that of the positive iterates. By definition of $f$, the set $S \cap f^{-1}(S)$ consists of two horizontal rectangles $H_0$ and $H_1$, each with height $\frac{1}{\mu}$. The set $S \cap f^{-1}(S) \cap f^{-2}(S)$ will then consist of four horizontal rectangles, each with height $\frac{1}{\mu^2}$, see Figure 7.5.

Again in an analogous way to the positive iterates, we can introduce a label system which keeps track of all the negative iterations.

We end up with with an infinite number of horizontal lines, each with an unique label of 0's and 1's. Finally, we obtain the invariant set of the SHM by taking the intersection of the positive and negative
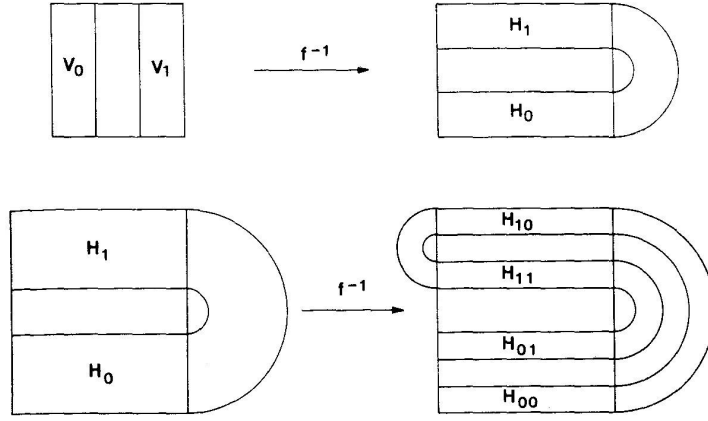
Figure 7.5: Negative iterates[11]

iterates:

$$\Lambda = \bigcap_{n=-\infty}^{\infty} f^n(S) = [\bigcap_{n=-\infty}^{0} f^n(S)] \cap [\bigcap_{n=0}^{\infty} f^n(S)]. \tag{7.4}$$

This set consists of the intersections between the horizontal and vertical lines obtained from the negative and positive iterates respectively. Furthermore each point $p \in \Lambda$ can be labeled uniquely by a bi-infinite sequence of 0's and 1's, which is obtained by concatenating the labels of the associated horizontal and vertical line. Let $s_{-1}..s_{-k}..$ be an infinite sequence of 0's and 1's ; then $V_{s_{-1}..s_{-k}..}$ corresponds to an unique vertical line. Likewise, a sequence $s_0..s_k..$ gives rise to an unique horizontal line defined by $H_{s_0..s_k..}$. A point $p \in \Lambda$ is an unique intersection point of a vertical and a horizontal line. We define the labeling map $\phi$:

$$\phi(p) \rightarrow ..s_{-k}..s_{-1}s_0..s_k... \tag{7.5}$$

Because of the way we have defined the labeling system, we have:

$$V_{s_{-1}..s_{-k}..} = \{p \in S | f^{-i+1}(p) \in V_{s_{-i}}, i = 1, 2, ..\}; \ H_{s_0..s_k..} = \{p \in S | f^i(p) \in H_{s_i}, i = 0, 1, ..\}. \tag{7.6}$$

And since $f(H_{s_i}) = V_{s_i}$, we get:

$$p = V_{s_{-1}..s_{-k}..} \cap H_{s_0..s_k..} = \{p \in S | f^i(p) \in H_{s_i}, i = 0, \pm 1, \pm 2, ..\}. \tag{7.7}$$

Hence, the way we have defined our labeling system (reflecting the dynamics of the rectangles under the different iterations) not only gives us a unique label for every $p \in \Lambda$, it also gives us information about the behavior of $p$ under iteration of $f$. To be more precise, the $s_k$th element in the bi-infinite sequence which represents $p$, indicates that $f^k(p) \in H_{s_k}$. As a result of this, we can easily obtain the representation for $f^k(p)$ from the representation of $p$. Let $p$ be represented (labeled) by $...s_{-k}...s_{-1}.s_0...s_k...$, where the decimal point between $s_{-1}$ and $s_0$ indicates the separation between the infinite sequence associated to the positive (future) and negative (past) iterations of $f$. We can now easily get the representation of $f^k(p)$ by shifting the decimal point $k$ places to the right if $k$ is positive, or $k$ places to the left if $k$ is negative. We formally do this by defining the so-called shift map. This shift map $\sigma$ works on a bi-infinite sequence and takes the decimal point one place to the right. So, if we have a point $p \in \Lambda$, the label is given by $\phi(p)$ (according to equation (7.5)) and the label of any iterate of $p$, $f^k(p)$, is given by $\sigma^k(\phi(p))$. For all $p \in \Lambda$ and all $k \in \mathbb{Z}$ we have:

$$\sigma^k \circ \phi(p) = \phi \circ f^k(p). \tag{7.8}$$

This relationship between the iterations of $p$ under $f$ and the iteration of its label $\phi(p)$ under the shift map, makes it necessary to spend some attention to symbolic dynamics. In this symbolic dynamics, which we will discuss in the next chapter, the shift map plays an important role. We will explain more about the relation to the SHM in chapter 9.

# Chapter 8

# Symbolic dynamics

Let $\Sigma$ be the collection of all bi-infinite sequences with entries 0 or 1. An element $s$ from $\Sigma$ has the form: $s = \{\cdots s_{-n} \cdots s_{-1}.s_0 \cdots s_n \cdots\}, s_i \in \{0,1\} \forall i$.

We can define a metric $d(\cdot, \cdot)$ on $\Sigma$. Let $s, \bar{s} \in \Sigma$, then

$$d(s, \bar{s}) = \sum_{i=-\infty}^{\infty} \frac{\delta_i}{2^{|i|}}, \tag{8.1}$$

with $\delta_i = 0$ if $s_i = \bar{s}_i$ and $\delta_i = 1$ if $s_i \neq \bar{s}_i$. See [2] for the proof that this is indeed a metric.

Next, we define a bijective map from $\Sigma$ to itself, called the shift map, as follows:

$$s = \{\cdots s_{-n} \cdots s_{-1}.s_0 s_1 \cdots s_n \cdots\} \in \Sigma \mapsto \sigma(s) = \{\cdots s_{-n} \cdots s_{-1} s_0 . s_1 \cdots s_n \cdots\} \in \Sigma. \tag{8.2}$$

This shift map $\sigma$ acting on the space of bi-infinite sequences of 0's and 1's (i.e. $\Sigma$) has some very interesting properties, which we will now examine.

## 8.1 Periodic orbits of the shift map

First we remark that $\sigma$ has two fixed points, namely the sequence which consists of only zero's and the sequence which consists of only ones. Shifting the decimal point will yield the same sequence.

Next we consider the points $s \in \Sigma$ which periodically repeat after some fixed length. We will denote these kind of points as follows: $\{\cdots 101010.11010 \cdots\}$ is written as: $\{\overline{10.10}\}$; $\{\cdots 101101.101101 \cdots\}$ is written as $\{\overline{101.101}\}$ etc. These kind of points are periodic under iteration of $\sigma$. For example, consider the point given by the sequence $\{\overline{10.10}\}$. We have: $\sigma\{\overline{10.10}\} = \{\overline{01.01}\}$ and $\sigma^2\{\overline{10.10}\} = \sigma\{\overline{01.01}\} = \{\overline{10.10}\}$. Hence, the point $\{\overline{10.10}\}$ has an orbit of period two for $\sigma$. From this example, it is easy to see that all points in $\Sigma$ which periodically repeat after length $k$, have an orbit of period $k$ under iteration of $\sigma$. Since there is a finite number of possible blocks, consisting of 0's and 1's, of length $k$ for every fixed $k$, we see that there exists a countable infinity of periodic orbits. Since $k \in \mathbb{N}$, all periods are possible.

## 8.2 Nonperiodic orbits

As we have just shown, the elements of $\Sigma$ which periodically repeat after some fixed length, correspond to periodic orbits under iteration of the shift map $\sigma$. Likewise, the elements of $\Sigma$ which consist of a nonrepeating sequence, correspond to nonperiodic orbits of $\sigma$. Suppose $s \in \Sigma$ is a nonrepeating sequence, then there's no $k \in \mathbb{N}$ such that $\sigma^k(s) = s$, because $s$ is nonrepeating. Hence the orbit of this $s$ under $\sigma$ is nonperiodic.

There is an uncountable infinite number of nonperiodic orbits. To see this, we will show that there

is an analogue between the cardinality of nonperiodic orbits of $\sigma$ and the cardinality of the irrational numbers in the closed interval $[0, 1]$ (which in turn has the same cardinality as $\mathbb{R}$), namely an uncountable infinity.

First, we notice that we can simply associate the bi-infinite sequence $s$ to a simple infinite sequence of zero's and one's, say $s'$ as follows: $s = \{\cdots s_{-n} \cdots s_{-1}.s_0 s_1 \cdots s_n \cdots\} \rightarrow s' = \{s_0 s_1 s_{-1} s_2 s_{-2} \cdots\}$. We also know that we can express every number in the interval $[0, 1]$ as a binary expansion (by rewriting the decimal notation in base 2). The binary expansions which don't have a repeating sequence correspond to the irrational numbers in the interval, because a repeating sequence would mean that we have a rational number. Hence, the bi-infinite sequences in $\Sigma$, which are nonrepeating, have a one-to-one correspondence to the irrational numbers in the interval $[0, 1]$ and therefore, have the same cardinality.

## 8.3 Dense orbit

Finally, we will show that there exists a $s \in \Sigma$ whose orbit is dense in $\Sigma$. An element $s \in \Sigma$ has a dense orbit in $\Sigma$ if for any given $s' \in \Sigma$ and $\varepsilon > 0$, there exists some integer $n$ such that $d(\sigma^n(s), s') < \varepsilon$, where $d(\cdot, \cdot)$ is the metric as defined in expression (8.1). We will prove the existence of such an $s$ by constructing it explicitly.

There are $2^k$ different sequences of 0's and 1's of length $k$. We can define an ordering of finite sequences as follows: consider two finite sequences, consisting of 0's and 1's, $x = \{x_1 \cdots x_k\}$ and $y = \{y_1 \cdots y_l\}$, having length $k$ and $l$ respectively. We will then say that $x < y$ if $k < l$. If $k = l$, then $x < y$ if $x_i < y_i$, where $i$ is the first integer such that $x_i \neq y_i$. For example, using this ordering, we have: $\{101\} < \{0000\}, \{110\} < \{111\}$. There are $2^1 = 2$ sequences of length 1 and we can put them in the right order: $\{0\}, \{1\}$. There are $2^2 = 4$ sequences of length 2 and the right order is: $\{00\}, \{01\}, \{10\}, \{11\}$. Define a finite sequence of length $p$ as $s_p^q$, where $1 \leq q \leq 2^p$ denotes its place in the ordering of sequences with length $p$. Now we will construct a bi-infinite sequence $s$ as follows: $s = \{\cdots s_4^2 s_2^2 s_2^1 . s_1^1 s_1^2 s_3^2 \cdots\}$. This bi-infinite sequence thus contains all possible sequences of any fixed length and we also know where a particular sequence is placed.

Our claim is that this particular $s$ is the bi-infinite sequence we were looking for, i.e. the orbit of this $s$ under $\sigma$ is dense in $\Sigma$. To see this, we must take a closer look at the metric. From the definition of this metric, it can be seen that the distance between two sequences is small when these two sequences have a central block (around the decimal point in the middle) which is identical. Suppose that two sequences $u$ and $v$ in $\Sigma$ have a central block of length $2l$ which is completely identical. Hence, for $-l \leq i \leq l$ we have that: $u_i = v_i$. The distance between $u$ and $v$ is given by:

$$d(u, v) = \sum_{i=-\infty}^{\infty} \frac{\delta_i}{2^{|i|}} = \sum_{i=-\infty}^{-l-1} \frac{\delta_i}{2^{|i|}} + \sum_{i=-l}^{l} \frac{\delta_i}{2^{|i|}} + \sum_{i=l+1}^{\infty} \frac{\delta_i}{2^{|i|}} = \sum_{i=-\infty}^{-l-1} \frac{\delta_i}{2^{|i|}} + 0 + \sum_{i=l+1}^{\infty} \frac{\delta_i}{2^{|i|}}. \quad (8.3)$$

When the central identical block gets larger, the distance between the two sequences becomes smaller, since the factor $2^{|i|}$ in the remaining part of the summation gets huge. In fact, the distance between $u$ and $v$ will approach zero as the length of the central identical block approaches infinity, since $\lim_{i \to \infty} \frac{i}{2^i} = 0$.

Now we return to our constructed $s$ and proof the claim. Let $s'$ be any bi-infinite sequence in $\Sigma$ and let $\varepsilon > 0$ be given. We have to show that there is an $n$ such that $d(\sigma^n(s), s') < \varepsilon$. Well, we have just seen that if we have a bi-infinite sequence, say $s''$, which has a big enough central block identical to that of $s'$, the distance $d(s', s'')$ will approach zero. It depends on $\varepsilon$ how large the identical block has to be, but we are guaranteed that $d(s', s'') < \varepsilon$ if the central identical block of $s''$ is long enough. Suppose that this central identical block has length $L$. The point now is that this central identical block of $s'$ and $s''$, consisting of a sequence of 0's and 1's of length $L$, occurs somewhere in $s$. This is a direct result of the way we have constructed $s$. All possible sequences of any fixed length are contained in $s$. Moreover, by the systematic way we have constructed $s$, we also know where a certain sequence is situated. If we now apply the shift map the appropriate number of times, say $n$, we can move the sequence we need to the center: $\sigma^n(s)$ will have the same central block as $s'$ and hence $d(\sigma^n(s), s') < \varepsilon$, which proves the claim.

# Chapter 9

# Dynamics in the homoclinic tangle

We will now show how the dynamics in the homoclinic tangle from Figure 6.3, the Smale Horseshoe Map (SHM) and the symbolic dynamics are related to eachother.

First, we focus on the relation between the dynamics of the shift map $\sigma$ on the collection of bi-infinite sequences $\Sigma$ and the dynamics of the SHM $f$ on its invariant set $\Lambda$. Remember that, in section 7.2, we have introduced the labeling map $\phi$ (7.5). It can be shown that $\phi$ is invertible and continuous [11]. Therefore, the relation (7.8) can be written as:

$$\phi^{-1} \circ \sigma^k \circ \phi(p) = f^k(p). \tag{9.1}$$

In other words, the map $\phi : \Lambda \to \Sigma$ is a homeomorphism, which means that the entire orbit structure of $f$ on $\Lambda$ is identical to that of $\sigma$ on $\Sigma$. So, the SHM $f$ has an invariant set $\Lambda$, such that:

- $\Lambda$ contains a countable set of periodic orbits of arbitrarily long periods.

- $\Lambda$ contains an uncountable set of nonperiodic orbits.

- $\Lambda$ contains a dense orbit.

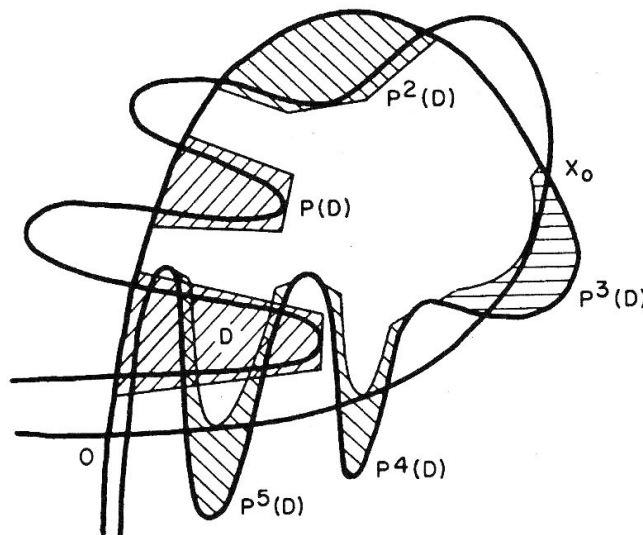The link between the SHM and the homoclinic tangle is illustrated in Figure 9.1. The basic idea is



Figure 9.1: Smale Horseshoe in the homoclinic tangle[8]

that, if we take a high enough iterate of the Poincaré map $P_\varepsilon$, a square $D$ close to the fixed point 0 is mapped into itself in exactly the same manner as in the SHM. For a rigorous proof we refer to Wiggins [11].

# Chapter 10

# Possible chaotic behavior of the coupled system

In the Chapters 6, 7, 8 and 9 we have shown that by using Melnikov's theory, we can determine whether a dynamical system contains a transverse homoclinic orbit, leading to a Smale Horseshoe Map in the homoclinic tangle.

We now return to system (4.5) and will examine the possibility of chaotic behavior. First, we show that we are allowed to use the Melnikov theory here, by checking all the necessary assumptions from section 5.1.

We can rewrite system (4.5) into the same form as system (5.1) by introducing the Hamiltonian function $H(A, z)$:

$$H(A, z) = \frac{1}{2}z^2 - \frac{1}{2}A^2 + \frac{1}{4}A^4. \tag{10.1}$$

System (4.5) can now be written as:

$$\begin{cases} A_x = \frac{\partial H}{\partial z}(A, z) + \mu g_1(A, z, x, \mu) \\ z_x = -\frac{\partial H}{\partial A}(A, z) + \mu g_2(A, z, x, \mu) \end{cases}, \tag{10.2}$$

where $g_1(A, z, x, \mu) = 0$ and $g_2(A, z, x, \mu) = -A(K_1 \sin x\sqrt{c} + K_2 \cos x\sqrt{c})$. Although the variables are different, system (10.2) is clearly of the same form as system (5.1). System (10.2) is sufficiently differentiable on the region of interest. The phase plane, as drawn in Figure 4.4, shows that the unperturbed system possesses a hyperbolic fixed point, connected to itself by a homoclinic orbit and that the region of the phase plane which is enclosed by the homoclinic orbit possesses a continuous family of periodic orbits. As remarked in section 4.2, the solution of the homoclinic orbit can be determined explicitly and is given by:

$$q_0(x) = (A_0(x), z_0(x)) = (\sqrt{2}\text{sech}(x), -\sqrt{2}\text{sech}(x)\tanh(x)). \tag{10.3}$$

The last necessary assumption is that the perturbation function $g = (g_1, g_2)$ is periodic in $x$. The null function $g_1$ is trivially periodic. The function $g_2$ appears to be periodic when looking at the sine and cosine terms, but there is a slight complication because of the multiplication by $A$ (containing the sech($x$) term). Strictly speaking, this makes the function $g_2$ non periodic. However, since $\mu \ll 1$, we can nevertheless use the Melnikov theory here [10].

Since all necessary assumptions from section 5.1 are satisfied, we are allowed to use the Melnikov theory for system (10.2). The Melnikov function as defined in expression (5.24) can now be calculated:

$$M(x_0, \phi_0) = \int_{-\infty}^{\infty} (DH(q_0(x)) \cdot g(q_0(x), x\sqrt{c} + x_0\sqrt{c} + \phi_0, 0))dx$$

$$= \int_{-\infty}^{\infty} (\frac{\partial H}{\partial A}(q_0(x)), \frac{\partial H}{\partial z}(q_0(x))) \cdot (g_1(q_0(x), x\sqrt{c} + x_0\sqrt{c} + \phi_0, 0), g_2(q_0(x), x\sqrt{c} + x_0\sqrt{c} + \phi_0, 0))dx$$

$$= \int_{-\infty}^{\infty} 2\text{sech}^2(x)\tanh(x)(K_1\sin\left(x\sqrt{c}+x_0\sqrt{c}+\phi_0\right)+K_2\cos\left(x\sqrt{c}+x_0\sqrt{c}+\phi_0\right))dx. \qquad (10.4)$$

As we have seen in section 6.1, variation of $\phi_0$ or $x_0$ are equivalent. Therefore, we will only consider the dependency with respect to $x_0$:

$$M(x_0) = \int_{-\infty}^{\infty} (2\text{sech}^2(x)\tanh(x))(K_1\sin\left(x\sqrt{c}+x_0\sqrt{c}\right)+K_2\cos\left(x\sqrt{c}+x_0\sqrt{c}\right))dx. \qquad (10.5)$$

The derivative of the Melnikov function (10.5) with respect to $x_0$ is:

$$\frac{d}{dx_0}M(x_0) = \int_{-\infty}^{\infty} (2\text{sech}^2(x)\tanh(x))(K_1\sqrt{c}\cos\left(x\sqrt{c}+x_0\sqrt{c}\right)-K_2\sqrt{c}\sin\left(x\sqrt{c}+x_0\sqrt{c}\right))dx. \qquad (10.6)$$

In order to check the existence of a transverse homoclinic orbit of system (10.2), we want to know if there exists a $x_0 \in [0, \frac{2\pi}{\sqrt{c}})$, such that $M(x_0) = 0$ and $\frac{d}{dx_0}M(x_0) \neq 0$.

First, we note that $\text{sech}^2(x)\tanh(x)$ is odd in $x$. Furthermore, we have:

$$K_1\sin\left(x\sqrt{c}+x_0\sqrt{c}\right)+K_2\cos\left(x\sqrt{c}+x_0\sqrt{c}\right)$$

$$= \sin x\sqrt{c}(K_1\cos x_0\sqrt{c}-K_2\sin x_0\sqrt{c})+\cos x\sqrt{c}(K_1\sin x_0\sqrt{c}+K_2\cos x_0\sqrt{c}). \qquad (10.7)$$

The $\sin\left(x\sqrt{c}\right)$ part is odd in $x$ and the $\cos\left(x\sqrt{c}\right)$ part is even in $x$. Since the odd part of the integrant of (10.5) will integrate to zero, we get:

$$M(x_0) = \int_{-\infty}^{\infty} (2\text{sech}^2(x)\tanh(x))(\sin x\sqrt{c})(K_1\cos x_0\sqrt{c}-K_2\sin x_0\sqrt{c})dx$$

$$= 2(K_1\cos x_0\sqrt{c}-K_2\sin x_0\sqrt{c})\int_{-\infty}^{\infty}\text{sech}^2(x)\tanh(x)\sin\left(x\sqrt{c}\right)dx. \qquad (10.8)$$

Using the method of residues, we find:

$$\int_{-\infty}^{\infty}\text{sech}^2(x)\tanh(x)\sin\left(x\sqrt{c}\right)dx = \frac{-\pi c\sinh(\frac{\pi}{2}\sqrt{c})}{1-\cosh(\pi\sqrt{c})}. \qquad (10.9)$$

Since this is strictly positive for $c > 0$, we see that all possible zeroes of the Melnikov function are found if:

$$(K_1\cos x_0\sqrt{c}-K_2\sin x_0\sqrt{c}) = 0,$$

or, on the interval $[0, \frac{2\pi}{\sqrt{c}})$ :

$$x_0 = \xi = \frac{1}{\sqrt{c}}\arctan\frac{K_1}{K_2}. \qquad (10.10)$$

Now we turn to the derivative of the Melnikov function (10.6). Substituting $x_0 = \xi$ from (10.10), we get:

$$\frac{d}{dx_0}M(x_0)|_{x_0=\xi} = -2\sqrt{c}\frac{K_1^2+K_2^2}{K_2\sqrt{\frac{K_1^2+K_2^2}{K_2^2}}}\int_{-\infty}^{\infty}\text{sech}^2(x)\tanh(x)\sin\left(x\sqrt{c}\right)dx. \qquad (10.11)$$

We have already mentioned that the integral (10.9) has no zero points for $c > 0$. The term containing $K_1$ and $K_2$ is also nonzero for all $K_1, K_2 \neq 0$ (i.e. for all nontrivial solutions of the $B$-equation (4.3)). Finally, since the term $-2\sqrt{c}$ is also nonzero for all $c > 0$, we can conclude that the derivative of the Melnikov function (10.11) is not equal to zero for $x_0 = \xi$.

We have thus found a value for $x_0$ (10.10) for which we will have a transverse homoclinic orbit, leading to chaos.

# Chapter 11

# Conclusion and suggestions

We have analyzed the possibility of chaotic behavior of system (1.1). In doing so, we made several assumptions which simplified this system. We only considered stationary solutions, so that the derivatives with respect to $t$ equal zero. All parameters have been assumed to be real valued and for the function $G$ we took: $G(B, \frac{\partial B}{\partial x}, |A|^2) := \beta_2 B$. Rescaling then yields system (3.5), where $c = \frac{\beta_2}{\beta_1}|\frac{\alpha_1}{\alpha_2}|$ and the plus or minus signs depend on the choice of $\alpha_i$ and $\beta_j$.

After uncoupling system (3.5) by setting $\mu = 0$, we showed that the phase plane of the $A$-equation contains a homoclinic orbit for $\frac{\alpha_2}{\alpha_1}, \frac{\alpha_3}{\alpha_2} < 0$ (i.e. case 2b from section 4.2). When the system is recoupled by setting $\mu \neq 0$, the homoclinic orbit will break open and we recalled the Melnikov theory to measure the distance between the manifolds. If the Melnikov function equals zero and its derivative is nonzero, the system will exhibit chaotic behavior. Since the Melnikov theory is only applicable to periodic perturbations, we took $c > 0$, or equivalently $\frac{\beta_2}{\beta_1} > 0$, so that the $B$-equation is periodic. We found a value for which the Melnikov function equals zero, while its derivative is nonzero and therefore can conclude that, for $\frac{\alpha_2}{\alpha_1}, \frac{\alpha_3}{\alpha_2} < 0$ and $\frac{\beta_2}{\beta_1} > 0$, system (3.5) exhibits chaotic behavior.

As mentioned before, we have made several assumptions in order to simplify the original system (1.1). Making all these assumptions less strict, would be the next step in the analysis. We could start with taking a slightly more complicated $B$-equation. If the solution of the modified $B$-equation is periodic, we can again use the Melnikov theory. It will become increasingly difficult though to find an analytic expression for the Melnikov function. Numerical calculations might be necessary in that case. If we make the $G$-function also dependent on $A$, it won't be possible anymore to consider the $B$-equation separately from the $A$-equation and things will get much more complicated.

We have only considered stationary solutions of system (1.1). As we have seen, these stationary solutions may exhibit chaotic behavior and it would be interesting to analyze the behavior of the non-stationary solutions. Unfortunately however, there are no (or not yet) suitable techniques available to do this.

A final suggestion for further analysis is to look at the complex case. What will happen if both the coefficients and the amplitudes will be complex instead of real valued?

Several of these suggestions have already been considered in [3, 4, 6] and we refer to these articles for a further analysis of system (1.1).

# Bibliography

[1] I. Aranson, L. Kramer , The world of the Ginzburg-Landau equation, Rev. Modern Phys. 74(2002) 99-143.

[2] R.L. Devaney, An Introduction to Chaotic Dynamical Systems, Benjamin/Cummings: Menlo Park, CA.

[3] A. Doelman, G. Hek, N.J.M. Valkhoff, Algebraically decaying pulses in a Ginzburg-Landau system with a neutrally stable mode, Nonlinearity 20(2007) 357-389.

[4] A. Doelman, G. Hek, N. Valkhoff, Stabilization by slow diffusion in a real Ginzburg-Landau system, J. Nonlinear Sci. 14(2004) 237-278.

[5] B. Dressel, A. Joets, L. Pastur, W. Pesch, E. Plaut, R. Ribotta, Competition of periodic and homogeneous modes in extended dynamical systems, Phys. Rev. Lett. 88(2)(2002) 024503.

[6] G. Hek, N. Valkhoff, Pulses in a complex Ginzburg-Landau system: Persistence under coupling with slow diffusion, Physica D 232(2007) 62-85.

[7] N.L. Komarova, A.C. Newell, Nonlinear dynamics of sand banks and sand waves, J. Fluid Mech. 415(2000) 285-321.

[8] L.Perko, Differential Equations and Dynamical Systems, Springer-Verlag, New York, 2001

[9] H. Riecke, Self-trapping of traveling-wave pulses in binary mixture convection, Phys. Rev. Lett. 68(1992) 301-304.

[10] C. Robinson, Sustained resonance for a nonlinear system with slowly varying coefficients, SIAM J. Math. An. 14(1983) 847-960.

[11] S. Wiggins, Introduction to Applied Nonlinear Dynamical Systems and Chaos, Springer-Verlag, New York, 1990